# Turbulent Flow between a Rotating Disk and a Parallel Wall

PAUL COOPER*
*TRW Inc., Cleveland, Ohio*
AND
ELI RESHOTKO†
*Case Western Reserve University, Cleveland, Ohio*

**A scalar effective viscosity method is used to calculate the incompressible flow in the gap between two infinite, parallel smooth disks, one of them rotating and the other stationary. The flow is calculated for two values of the gap Reynolds number $\omega s^2/\nu$, namely 296 and 2852, where $\omega$ is the disk angular velocity, $s$ the gap width, and $\nu$ the kinematic viscosity of the fluid; and over a range of radial Reynolds number $\omega r^2/\nu$ from 0 to $10^7$ where $r$ is the radius from the axis of rotation. A numerical shooting technique is used to match the two boundary-layer flows arising on the disk and wall. Gradual transition is assumed over the range $1.6\times10^5 \leq \omega r^2/\nu \leq 2.5\times10^5$. The results are in good agreement with Daily and Nece's measurements of velocity profiles and disk friction drag for enclosed rotating disks, and at sufficiently large radius the local skin friction approaches that of turbulent Couette flow.**

## Nomenclature

| | |
|---|---|
| $a$ | = maximum radius of disk |
| $c_{f,\theta}$ | = local circumferential coefficient of friction on disk, Eq. (32) |
| $C_m$ | = integrated disk friction moment coefficient, Eq. (33) |
| $f$ | = radial stream function, Eq. (18) |
| $g$ | = circumferential stream function, Eq. (19) |
| $k_v$ | = switching factor for eddy viscosity, Eq. (14) |
| $l$ | = Prandtl's mixing length |
| $M$ | = integrated disk friction moment, Eq. (34) |
| $p$ | = pressure |
| $\hat{p}$ | = dimensionless pressure, Eq. (30) |
| $r$ | = radial distance from axis of rotation |
| $r_e$ | = dimensionless radius $[=(R_e)^{1/2}]$ |
| $R_e$ | = radial Reynolds number $(=\omega r^2/\nu)$ |
| $R_{e,s}$ | = gap width Reynolds number $(=\omega s^2/\nu)$ |
| $s$ | = gap width |
| $u, v, w$ | = mean radial, circumferential and axial velocity components, respectively |
| $U$ | = relative circumferential velocity defect |
| $\mathbf{u}$ | = mean velocity vector parallel to disk and wall |
| $\langle u'w'\rangle\ \langle v'w'\rangle$ | = Reynolds stresses (time averages of $u'w'$ and $v'w'$) |
| $z$ | = axial distance from disk |
| $\tilde{z}$ | = axial distance from nearer boundary (disk or wall) |
| $\beta$ | = dimensionless pressure gradient, Eq. (22) |
| $\gamma$ | = intermittency factor |
| $\delta$ | = boundary-layer thickness |
| $\eta$ | = dimensionless axial distance from disk, Eq. (17) |
| $\theta$ | = circumferential coordinate = central angle |
| $\nu$ | = kinematic viscosity |
| $\rho$ | = fluid density |
| $\tau$ | = shear stress |
| $\omega$ | = angular speed of disk |

*Subscripts*

| | |
|---|---|
| $b$ | = boundary (wall or disk) |
| $d$ | = disk |
| $e$ | = effective |
| inner | = inner layer (next to boundary) |
| outer | = outer layer |
| o.d. | = maximum radial position on disk |
| $r$ | = radial component |
| $t$ | = turbulent (eddy viscosity) |
| $tr$ | = transition—at minimum radius of transition range |
| $tr,b$ | = transition—at maximum radius of transition range |
| $0$ | = circumferential component |
| $\infty$ | = outside boundary layer |

*Superscripts*

| | |
|---|---|
| $'$ | = fluctuating component ($u$, $v$, and $w$ only) |
| $,$ | = partial differentation with respect to $\eta$ (except $u$, $v$ and $w$) |
| $+$ | = divided by $\nu$ |

## Introduction

THE configuration of a disk rotating near a coaxial, stationary disk (herein called a "wall") is frequently encountered, e.g., in fluid machinery; and information about the attendant resistance to rotation is often sought. As indicated in Fig. 1, the flow in the gap is typically turbulent. Daily and Nece,[1] who performed extensive experimental work on enclosed disks with various gap widths, inferred that laminar flow exists at the inner radii of the gap. This was in fact observed in the flow next to a "free" disk, i.e., one rotating far from any stationary wall.[2]

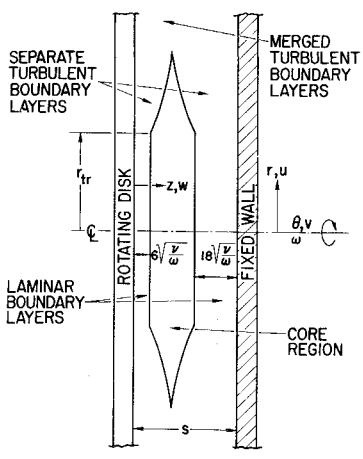


**Fig. 1 Structure of the flowfield in the gap between a rotating disk and a parallel fixed wall, showing the cylindrical coordinate system used. For a sufficiently small gap width $s$, the boundary layers are merged.**

Received March 22, 1974; revision received October 8, 1974. This research was supported by NASA Grant NGR 36-003-139, under the technical cognizance of W. R. Britsch.

Index categories: Viscous Nonboundary-Layer Flows; Boundary Layers and Convective Heat Transfer—Turbulent.

* Principal Engineer, Power Accessories Division.

† Professor of Engineering and Head, Department of Fluid, Thermal, and Aerospace Sciences, School of Engineering. Associate Fellow AIAA.

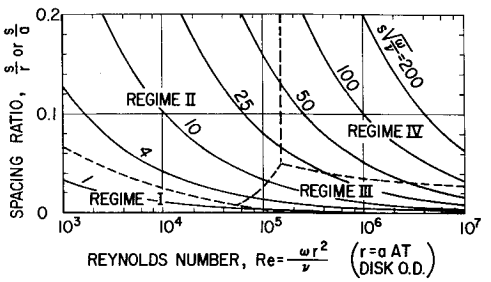


**Fig. 2 Approximate gap flow regimes for enclosed rotating disks. Adapted from Ketola and McGrew.[7] The regimes in a given configuration of gap width $s$ and radius $a$ are found along a line of constant $s(\omega/\nu)^{1/2}$ for $r \leq a$.**

Precise theoretical analyses of laminar flow in radially infinite gaps have been conducted[3-5] yielding radial and circumferential velocity components $u$ and $v$ proportional to radius $r$ and constant axial velocity $w$. For sufficiently large gap width $s$, two boundary layers of the constant thicknesses noted on Fig. 1 exist separately with an intervening core of fluid rotating at 0.3135 of the disk angular speed $\omega$.

Where a cylindrical enclosure is placed around the gap, Bondor[6] showed that the laminar flowfield is negligibly affected except in a small region at the maximum radius of the gap. Furthermore, he found no net difference in the fluid drag torque on the disk from that calculated using infinite-disk results. Therefore, in order to simplify the problem, the gap is here assumed to be infinite in radial extent for all flows.

The radially similar behavior of laminar gap flow is absent in turbulent fields, the boundary layers thickening with $r$ greater than an assumed transition radius $r_{tr}$, as shown in Fig. 1. For sufficiently large $r$, the turbulent layers will be merged. The possible flow regimes that can exist in the gap were identified by Daily and Nece[1] as follows: Regime I—merged laminar boundary layers that produce a disk shear stress $\tau_d$ varying inversely with spacing $s$; Regime II—separate laminar layers (and merged ones that also produce negligible dependence of $\tau_d$ on $s$); Regime III—merged turbulent boundary layers; and Regime IV separate turbulent boundary layers.

The approximate domains for which these flow regimes exist are shown in Fig. 2 in terms of the spacing ratio $s/a$ and radial Reynolds number $\omega a^2/\nu$, where $a$ is the maximum radius of the disk. Ketola and McGrew[7] deduced this from the data of Daily and Nece.[1] If it is assumed that the results for a disk of maximum radius $a$ apply equally well to the inward portion of a larger disk, the local radius $r$ may be substituted for $a$. Then the domains of these regimes in any particular gap can be identified by the location of the applicable line of constant dimensionless gap width $s(\omega/\nu)^{1/2}$. For example, if this width is 10, only Regimes II and III exist in the gap. But, for any width, Regime III is always attained at sufficiently large radius.

A comprehensive analytical approach to gap flows should apply to all these regimes. Bayley and Owen[8] analyzed the turbulent regimes for the case of superimposed radial outflow. They made eddy-viscosity substitutions for the two Reynolds stress terms in the boundary-layer equations. This approach, together with an assumption about the radial location of transition, was successfully employed to describe the boundary-layer flow due to a free disk.[9] Therefore, an effective viscosity method is here applied to infinite gaps involving Regimes II, III, and IV with zero net radial through-flow.

## Method of Analysis

In the fixed $r-\theta-z$ coordinate system indicated in Fig. 1, $u$, $v$ and $w$ are the associated mean absolute velocity components. While the fluid moves circumferentially ($v$) in the gap, it is also thrown radially outward ($u$) by the disk and flows inward along the wall, the circuit being completed by an axial feeding of the fluid across the gap from the wall layer to the disk layer ($-w$). Thus near disk and wall, the velocity vectors form the skewed profiles typical of three-dimensional boundary layers.

### Equations of Motion

The turbulent boundary-layer equations for steady, incompressible, axisymmetric flow are therefore applied to the entire gap flow. The core, if any, is assumed to be devoid of any motion (such as a net radial throughflow) that would invalidate their applicability. First the continuity equation is

$$(1/r)[\partial(ur)/\partial r] + \partial w/\partial z = 0 \tag{1}$$

and the momentum equations are

$$u\partial u/\partial r - v^2/r + w\partial u/\partial z = -(1/\rho)\,dp/dr + \nu\partial^2 u/\partial z^2 - \partial\langle u'w'\rangle/\partial z \tag{2}$$

in the $r$-direction and

$$u\partial v/\partial r + uv/r + w\partial v/\partial z = \nu\partial^2 v/\partial z^2 - \partial\langle v'w'\rangle/\partial z \tag{3}$$

in the $\theta$-direction and

$$\partial p/\partial z = 0 \tag{4}$$

in the $z$-direction. As was done for the free disk case,[9] the two Reynolds stresses are assumed to be related to the mean velocity gradient as follows

$$\langle u'w'\rangle = -\nu_t\,\partial u/\partial z \tag{5}$$

and

$$\langle v'w'\rangle = -\nu_t\,\partial v/\partial z \tag{6}$$

where $\nu_t$ is a scalar kinematic eddy viscosity for turbulent flow. Equations (2) and (3) now become

$$u\partial u/\partial r - v^2/r + w\partial u/\partial z = -(1/\rho)\,dp/dr + (\partial/\partial z)(\nu_e\,\partial u/\partial z) \tag{7}$$

and

$$u\partial v/\partial r + uv/r + w\partial v/\partial z = (\partial/\partial z)(\nu_e\,\partial v/\partial z) \tag{8}$$

where the scalar effective kinematic viscosity

$$\nu_e = \nu + \nu_t \tag{9}$$

Thus the total apparent shear stress vector $\tau = \rho\nu_e\,\partial\mathbf{u}/\partial z$ has the same direction as the local velocity gradient parallel to the disk and wall.

### Effective Viscosity

The kinematic eddy viscosity $\nu_t$ is given by an adaptation of the two-layer model used by Cebeci and Smith for two-dimensional turbulent boundary layers.[10] Figure 3 illustrates the domains of the inner and outer portions of the turbulent layers, both of which are assumed to be laminar for $r < r_{tr}$. For the inner portion or layer, $\nu_t$ is given by

$$\nu_{t,\text{inner}} = 0.16\tilde{z}^2\left|\frac{\partial\mathbf{u}}{\partial z}\right|\{1-\exp[-\tilde{z}(|\tau_b|/\rho)^{1/2}/(26\nu)]\}^2 \tag{10}$$

where $\tilde{z}$ is the distance from the nearer boundary (disk or wall); $\tau_b$ is the shear stress vector at that boundary; and $\mathbf{u}$ is the velocity vector parallel to the boundaries, so that

$$|\partial\mathbf{u}/\partial z| = [(\partial u/\partial z)^2 + (\partial v/\partial z)^2]^{1/2} \tag{11}$$

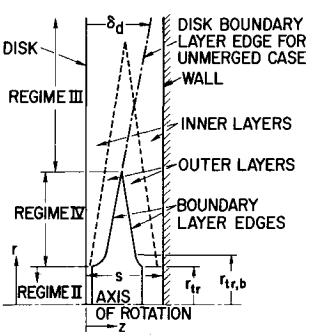


**Fig. 3 Elements of the gap boundary-layer structure that enter into the effective viscosity model. A gradual introduction of eddy viscosity is specified over the interval $r_{tr} \leq r \leq r_{tr,b}$.**

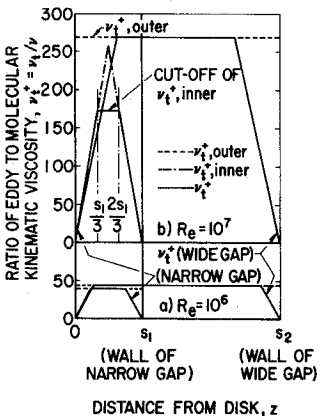


**Fig. 4 Typical eddy viscosity profiles for intermittency $\gamma = 1$. For $\gamma < 1$, $\nu_t$ drops to zero at edges of the boundary layers; i.e., in the middle of a wide gap.**

Equation (10) contains the Van Driest exponential factor. This approximates the behavior of $\nu_t$ in the sublayer region. Elsewhere, $\nu_t \to l^2 |\partial \mathbf{u}/\partial z|$ where $l = 0.4\,\tilde{z}$ is Prandtl's mixing length.

For the outer layer, $\nu_t$ is approximated by

$$\nu_{t,\text{outer}} = 0.057(|\tau_{\theta,d}|/\rho)^{1/2}\delta_d\gamma \tag{12}$$

an expression which is derived[12] from the concepts originally advanced by Clauser.[11] Equation (10) yields an increasing eddy viscosity with distance from the boundary, as illustrated in Fig. 4. Equation (12) is applied for $\tilde{z}$ greater than that at which both equations yield the same result—also shown in the figure.

The intermittency factor $\gamma$ in Eq. (12) was set equal to unity except in one case (to be noted) wherein the following expression was applied:

$$\gamma = 1/[1+5.5(\tilde{z}/\delta_d)^6] \tag{13}$$

The considerable difference in $\nu_{t,\text{outer}}$ arising from these two choices of $\gamma$ had little effect on the velocity and skin friction results. Thus it was reasonable to unify the $\nu_{t,\text{outer}}$-expressions for both disk and wall boundary-layer flows in terms of the disk-side data $\tau_{\theta,d}$ and $\delta_d$.

Furthermore since $\delta_d$ becomes a fictitious quantity when the boundary layers merge, (Regime III, Fig. 3) it was taken to be a linear combination of curve fits to two single boundary-layer solutions of the kind outlined in Ref. 9—one for $v = 0$ as $z \to \infty$ (the free disk case) and one for $v = \omega r/2$ as $z \to \infty$.[12]

Finally, for the case of merged inner layer—as occurs in narrow gaps or at large radii (Fig. 3)—the sharp peak in $\nu_t$ that would otherwise exist is avoided as shown in Fig. 4 by spanning the middle third of the gap by a straight-line distribution of $\nu_t$.

This model for $\nu_t$ is used because it is simple, convenient and because it gives good results in similar flows. Actually the two Reynolds stresses [Eqs. (5) and (6)] are intimately related to other turbulence quantities. For example, Bradshaw treats three-dimensional turbulent boundary layers by adding a differential transport equation for each Reynolds stress.[13] This does not remove the empiricism, but transfers it to the higher level of approximating the turbulent kinetic energy equations. Such an approach is also used by Koosinlin and Lockwood[14] in their analysis of swirling flows. As a consequence of their modeling, they found that the eddy viscosity near the wall is far from isotropic, but they acknowledge that good results on free rotating disks are also obtained for an eddy viscosity that is everywhere isotropic.

#### Transition

Transition from laminar flow ($\nu_t = 0$) at $r < r_{tr}$ to the flow just described was effected gradually over the range $r_{tr} \leq r \leq r_{tr,b}$ through a switching factor $k_\nu$, so that $\nu_t = k_\nu$ ($\nu_{t,\text{inner}}$ or $\nu_{t,\text{outer}}$) in that $r$-range. Here,

$$k_\nu = \{\exp[-6(1-x)^2] - e^{-6}\}/[1-e^{-6}] \tag{14}$$

where $x = (r-r_{tr})/(r_{tr,b}-r_{tr})$, providing a smooth variation of $k_\nu$ from 0 to 1 in this $r$-range that effects transition with the least numerical trauma. The range was determined by specifying $R_{e,tr} = 1.6\times10^5$ and $R_{e,tr,b} = 2.5\times10^5$. These choices were made because a) the boundary layer was observed to be fully turbulent on a free disk at $R_e = 3\times10^5$, b) the radially inward motion involved in gap flows can be expected to carry the turbulence to smaller radii, and c) drag moment data for enclosed disks[1] evidence transition approximately in the range chosen.

#### Boundary Conditions

With the foregoing effective viscosity model represented by Eq. (9), Eqs. (1), (4), (7), and (8) form a closed system of partial differential equations in $r$ and $z$ for the three velocity components $u$, $v$, and $w$, and the pressure $p$. The boundary conditions are that at the disk, where $z = 0$,

$$v = \omega r, \quad u = w = 0 \tag{15}$$

and at the wall, where $z = s$

$$u = v = w = 0 \tag{16}$$

The $r$-independent laminar solution yields the starting velocity profiles for turbulent flow at $r = r_{tr}$.

## Method of Solution

This system is solved by a) introducing a transformation that aids in the elimination of the continuity equation, b) expressing the partial derivatives with respect to $r$ in finite difference form, and c) matching solutions for each side of the gap in a numerical shooting process. The calculations are conducted by advancing radially outward in steps, numerically integrating the equations axially from the boundaries and matching in the interior of the gap at each radial step or station. More rapid numerical methods for turbulent boundary layers are in use; e.g. the implicit finite difference approach.[9] In the gap flow however, the radial pressure and mid-gap velocity distributions are not specified (as in the usual boundary-layer problem), but are the result of matching the disk and wall layers. Attempts to utilize the more rapid approaches led to instabilities, particularly in the transition zone which turned out to be a region of rapidly varying pressure gradient.

#### Transformed Equations and Boundary Conditions

The transformation is defined as follows

$$z \to \eta; \quad r \to r$$

where

$$\eta = z(\omega/\nu)^{1/2} \tag{17}$$

Let

$$f'(\eta, r) = u/(\omega r) \tag{18}$$

and

$$g'(\eta, r) = v/(\omega r) \tag{19}$$

where the primes on the stream functions $f$ and $g$ denote partial differentation with respect to $\eta$. Correspondingly transformed, the continuity equation [Eq. (1)] is integrated, yielding the axial velocity component $w$

$$w/(\omega\nu)^{1/2} = -2f - r\partial f/\partial r \tag{20}$$

$w$ and $f$ having been set equal to zero at $\eta = 0$. By substituting this expression for $w$ in the momentum equations [Eqs. (7) and (8)], they transform to

$$(\nu_e{}^+ f'')' - \beta^2 + g'^2 - f'^2 + 2ff'' = r(f'\partial f'/\partial r - f''\partial f/\partial r) \tag{21}$$

for the $r$-direction with $\beta$, the dimensionless pressure gradient given by

$$\beta = [(dp/dr)/(\rho r\omega^2)]^{1/2} \tag{22}$$

and

$$(\nu_e{}^+ g'')' - 2f'g' + 2fg'' = r[f'(\partial g'/\partial r) - g''(\partial f/\partial r)] \tag{23}$$

for the $\theta$-direction, where

$$\nu_e{}^+ = \nu_e/\nu = 1 + \nu_t/\nu \tag{24}$$

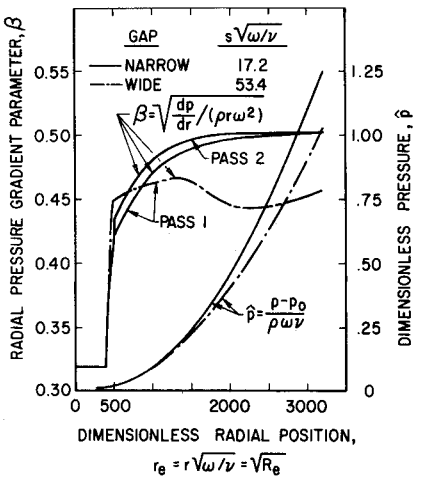


**Fig. 5 Pressure and pressure gradient. Pressure results for both passes of the narrow gap computations differ negligibly. A second pass of the wide gap computations was not conducted.**

The transformed inner and outer eddy viscosity relations [Eqs. (10) and (12)] are

$$\nu_{t,\text{inner}}^{+} = 0.16\tilde{\eta}^2[(R_e)(g''^2+f''^2)]^{1/2} \times \{1-\exp[(-\tilde{\eta}/26)(R_e)^{1/4}(g_b''^2+f_b''^2)^{1/4}]\}^2 \quad (25)$$

and

$$\nu_{t,\text{outer}}^{+} = 0.057(R_e)^{1/4}(|g_d''|)^{1/2}\delta_d(\omega/\nu)^{1/2}\gamma \quad (26)$$

These are utilized as previously described and illustrated in Fig. 4.

Equations (15–19) yield the transformed boundary conditions

$$\begin{aligned} &\eta = 0: \quad g' = 1; \quad f' = f = 0 \qquad \text{(at the disk)} \\ &\eta = s(\omega/\nu)^{1/2}: \quad g' = f' = f = 0 \qquad \text{(at the wall)} \end{aligned} \quad (27)$$

$f = 0$ at the wall as well as at the disk, because the net radial outflow in the gap at any $r$ is, using Eqs. (17) and (18),

$$0 = 2\pi r\int_o^s u\,dz = 2\pi(\omega\nu)^{1/2}r^2(f_w - f_d) \quad (28)$$

and $f_d = 0$ in the derivation of Eq. (20). It can be seen from Eqs. (21) and (23–26) that the laminar, similarity solution is obtained $r = 0$. The right-hand sides of Eqs. (21) and (23) and the $\nu_t$-relations [Eqs. (25) and (26)] produce the nonsimilar results of turbulent flow. The laminar results are the starting profiles at the specified transition radius.

### Numerical Procedure

At each radial position, Eqs. (21) and (23) were integrated numerically in the $\eta$-direction from each boundary. The fourth-order Runge-Kutta method was used at the three points nearest the boundaries thereby furnishing starter values for the more rapid fourth-order Adams-Moulton method.

At the matching point in the interior of the gap, continuity in the velocities and their first derivatives was required; which is satisfied by matching $f, f', g', f''$, and $g''$. Guesses of $\beta$ and of disk and wall values of $f''$ and $g''$ were required to start the $\eta$-integration at those boundaries, $f, f'$, and $g'$ being known there through the boundary conditions. These guesses had to be very precise in order to obtain this matching. They were obtained from the previous $r$-station, the innermost or laminar values having to agree very closely with the data of Refs. 3–5 in order to obtain a solution. These were improved in up to five interations at each $r$-station, this shooting process being repeated at each radial position.

The $r$-derivatives were expressed as finite differences of data from the current $r$-station ($n$) and the previous one ($n-1$)

$$\partial q/\partial r = [(q_n - q_{n-1})/(r_n - r_{n-1})] \quad (29)$$

with $q$ playing the role of $f, f'$, or $g'$. Application of this one-sided expression to various $r$ step-sizes showed that it had no effect on the results. However, numerical instabilities arose when the attempt was made to evaluate these radial partial derivatives in terms of the data of the current pass (of calculations over the radial range of the problem). This led to the multi-pass approach in which these derivatives were evaluated in terms of data from the preceding pass. The instability was apparently due to the variation of pressure gradient vs $r$ and the associated $r$-variation of the tangential velocity ratio $g'$ in the middle of the gap, particularly in the transition region. Since it was found that the nature (through various $k_v$ vs $r$ relations) and the extent of the transition region had no effect on the outer, turbulent region, only one pass was made in the region $r \leqq r_{tr,b}$. Furthermore, a complete omission of the second pass had a small effect on the velocity field and led to errors in disk friction drag no larger than 3%. Pass 1 yields the locally similar result, with zero for the radial partial derivatives. Thus the eddy viscosity formulas [Eqs. (25) and 26)] are far more important in determining the gap flow than is the history of its development at other radii.

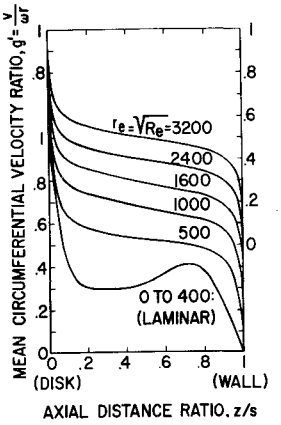


**Fig. 6 Calculated circumferential velocity profiles for turbulent flow (except as noted) in narrow gap. $s(\omega/\nu)^{1/2} = 17.2$; ($R_{e,s} = 296$).**

## Calculated Results

By means of the foregoing method, results were obtained for two values of dimensionless gap width $s(\omega/\nu)^{1/2}$, namely 17.2 and 53.4. These correspond to gap width Reynolds numbers $R_{e,s} = \omega s^2/\nu$ of 296 and 2852 and are called the "narrow" and "wide" gaps respectively. Computations covered the radial Reynolds number range $R_e = \omega r^2/\nu$ from 0–$10^7$ in both cases. Two passes of computations were made for the narrow gap—part of a third pass producing no change from the results of the second. Only one pass was made for the wide gap, due to the larger number of axial positions (570 vs 345 for the narrow gap) and consequent greater running time. In the light of the small differences between the results of the two passes of the narrow-gap solution, the wide-gap data for one pass are felt to be reasonable for that case.

The intermittency factor $\gamma$ [Eq. (13)] was applied in the outer eddy viscosity relation [Eq. (12)] in the wide-gap solution. Comparison with another such solution for $\gamma = 1$ showed little

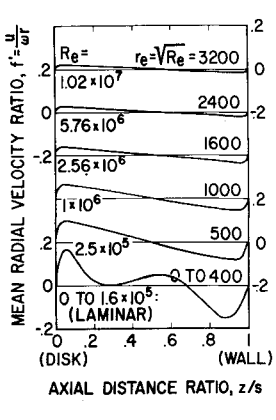


**Fig. 7 Calculated radial velocity profiles for turbulent flow (except as noted) in narrow gap. $s(\omega/\nu)^{1/2} = 17.2$.**

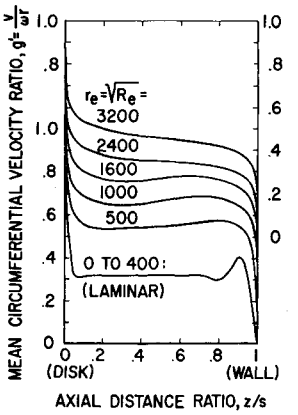


**Fig. 8 Calculated circumferential velocity profiles for turbulent flow (except as noted) in wide gap.** $(s(\omega/\nu)^{1/2} = 53.4;$ $(R_{e,s} = 2852).$

$\gamma$-effect on fluid shear stress at the disk and wall, while the velocity profiles in the middle of the gap showed less curvature for $\gamma = 1$ as might be expected for the greater resulting mid-gap eddy viscosity. Theoretical results for $\gamma < 1$ in the gap interior agreed best with available velocity profile measurements. The intermittency question did not arise for the narrow gap case, because Eq. (13) there gives values of $\gamma$ that differ negligibly from unity.

### Pressure and Pressure Gradient

The resulting radial distribution of the pressure gradient parameter $\beta$ [Eq. (22)] is shown in Fig. 5 for both gap widths. The laminar result is $\beta = 0.3135$ as expected,[5] since Fig. 2 shows both gaps to contain Regime II flow at low $R_e$ values. An increase of $\beta$ in the transition zone brings the $\beta$-values above 0.4 at the fully turbulent end of this zone. The largest differences between the respective results of the two passes exist in the region of significant $\beta$-variation, there being no difference at the high $R_e$ values where $\beta$ (and the mid-gap value of $g'$) levels off to a value slightly greater than $\frac{1}{2}$. For the wide gap, it is expected that $\beta$ would approach $\frac{1}{2}$ at sufficiently greater $R_e$—an asymptotic result to be discussed further on.

Integration of the $\beta$-distributions yields the pressure parameter $\hat{p} = (p - p_o)/(\rho\omega\nu)$ also shown in Fig. 5

$$\hat{p} = \int_o^{r_e} \beta^2 r_e \, dr_e \tag{30}$$

For both narrow-gap passes the results for $\hat{p}$ differed negligibly from each other.

### Velocity Profile

Figures 6–9 illustrate the development of the circumferential and radial velocity components vs Reynolds number for both gap widths. To aid in illustrating the radial development of the flow, these curves are presented in a staggered sequence; i.e., the origin for the velocity component profile at a given value of $r_e$ is displaced upward by one grid marking from that for the next lower $r_e$. As would be expected from consideration of the bulk

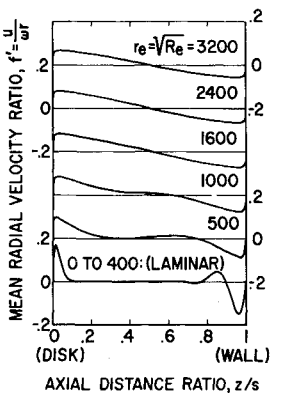


**Fig. 9 Calculated radial velocity profiles for turbulent flow (except as noted) in wide gap.** $s(\omega/\nu)^{1/2} = 53.4.$

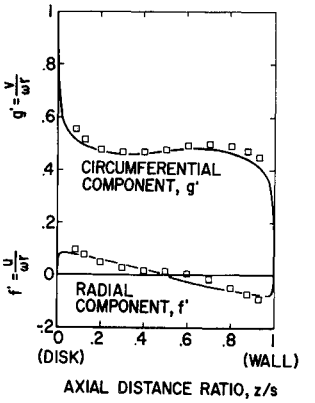


**Fig. 10 Comparison of turbulent mean velocity profiles from theory and experiment for wide gap.** $s(\omega/\nu)^{1/2} = 53.4;$ $(R_{e,s} = 2852).$ **Squares denote measurements[1]:** $R_{e,o.d.} = 4.4 \times 10^6;$ $R_e = 2.57 \times 10^6;$ $s/a = 0.0255.$ **Lines denote present theory:** $R_e = 2.56 \times 10^6.$

motion [Eqs. (2) and (22)], the values for $g'$ at the middle of the gap (Figs. 6 and 8) agree very closely with the corresponding $\beta$-values of Fig. 5.

In the terminology of Fig. 2, it is evident from Figs. 6 and 7 that the turbulent flow in the narrow gap is in Regime III (merged boundary layers), while that for the wide gap (Fig. 8 and 9) indicates the separate layers of Regime IV for $r(\omega/\nu)^{1/2} < 1600$, i.e. $R_e < 2.56 \times 10^6$, the layers being merged in a Regime III flow at greater $R_e$. The laminar flow in both gaps is that of Regime II. These observations are in agreement with Fig. 2, which was deduced from trends in the experimental data of Daily and Nece for the integrated drag moment coefficient of enclosed rotating disks[1]. Figure 10 compares the wide-gap results at $R_e = 2.56 \times 10^6$ with the corresponding set of velocity profiles obtained by Daily and Nece in that work. The good agreement demonstrates the success of the present calculation method and its applicability to configurations of finite radius. Further velocity profile comparisons could not be made as no other applicable experimental data were found.

### Disk Friction Drag

The local skin friction drag at the disk, $\tau_d$, is found from the velocity gradient there. The circumferential component of the skin friction $\tau_{\theta,d}$ is of interest as it contributes to the total drag moment $M$ of the fluid on the disk. This component is defined as follows

$$\tau_{\theta,d} = \rho\nu(\partial v/\partial z) = \rho\omega\nu(R_e)^{1/2} g_d'' \tag{31}$$

Results obtained for the coefficient of local circumferential disk friction $c_{f,\theta}$, where

$$c_{f,\theta} = \tau_{\theta,d}/(\rho\omega^2 r^2/2) \tag{32}$$

are presented in Fig. 11 for both the wide and narrow gaps.

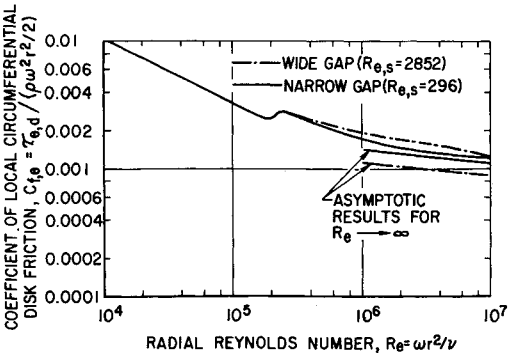


**Fig. 11 Calculated local skin friction coefficient at disk, $c_{f,\theta}$. Also shown are asymptotic results for infinite radial Reynolds number calculated from the law of the wall [Eq. (36)].**

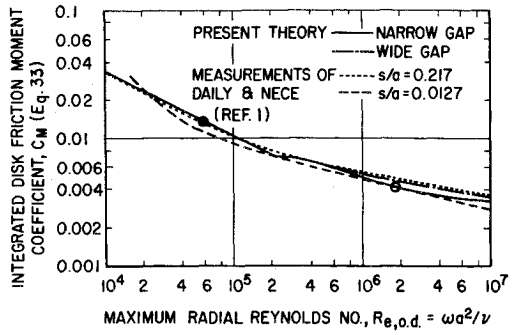


**Fig. 12 Integrated disk friction drag moment. Comparison of present theory for the wide and narrow gaps [constant $s(\omega/\nu)^{1/2} = 53.4$ and 17.2, respectively] with experimental data for enclosed rotating disks [constant $s/a$, but varying $s(\omega/\nu)^{1/2}$]. On each theoretical curve, a point is shown at which $s/a$ has the same value as does the nearer experimental curve.**

Figure 12 shows the results for integrated disk friction moment coefficient $C_m$, where

$$C_m = 2M/(\rho\omega^2 a^5/2) \tag{33}$$

with

$$M = \int_o^a 2\pi r^2 |\tau_{\theta,d}| dr \tag{34}$$

which applies to the entire disk surface radially inward of $r = a$. Also plotted on Fig. 12 are two of the experimental curves of Daily and Nece. Each of the latter applies however, to several gap-flow configurations, all having the same gap-to-radius ratio $s/a$; while each curve from the present theory applies to flows at various dimensionless radii $(R_{e,o.d.})^{1/2}$ at a constant dimensionless gap width $s(\omega/\nu)^{1/2}$. Where both the theoretical and experimental curves have the same $s/a$, agreement is achieved. These points are specially indicated in Fig. 12: The narrow gap has $s/a = 0.0127$ at $R_{e,o.d.} = 1.83 \times 10^6$ and the wide gap $s/a = 0.217$ at $R_{e,o.d.} = 6 \times 10^4$.

#### Asymptotic Behavior at Large Reynolds Number

At sufficiently large $R_e$, a simple relationship for the local drag coefficient $c_{f,\theta}$ is motivated by examination of the foregoing results. Specifically the radial velocity component is nearly suppressed in the narrow gap at $R_e = 10^7$ (Fig. 7), leading to the speculation that the fluid motion is essentially that of a two-dimensional, turbulent, Couette flow. In such a case, Eqs. (1–3) would reduce to $w = 0$, $u = 0$, and $(\partial/\partial z)(\nu_e \partial v/\partial z) = 0$ or $\tau_\theta = \rho\nu_e \partial v/\partial z = \tau_{\theta,d} = \tau_{\theta,w}$ and $\tau_r = 0$; $\nu_e$ being given by $\nu + \nu_{t,\text{inner}}$, [Eq. (10)]. The result of this problem should be the matching of two law-of-the-wall profiles[15] in the middle of the gap. From Coles' tabulation, one has approximately

$$v/v_\tau = [\ln(zv_\tau/\nu)]/0.4 + 5 \tag{35}$$

where $v_\tau = (\tau_\theta/\rho)^{1/2}$. At the match point $v = \omega r/2$ and $z = s/2$, and Eq. (35) can be rewritten, using Eq. (32), as follows

$$0.173718(2/c_{f,\theta})^{1/2} + \log_{10}(2/c_{f,\theta}) = \log_{10}(\omega s^2/\nu) + \log_{10}(R_e) + 1.13512 \tag{36}$$

Equation (36) is plotted on Fig. 11 for both gap widths. The narrow-gap curves approach each other at large $R_e$, and the wide-gap curves can be assumed to converge at $R_e > 10^7$: the wider the gap the greater the radius at which the asymptotic flow pattern develops.

## Summary and Conclusions

The laminar and turbulent, incompressible, steady flow in the gap between a rotating disk and a fixed, parallel wall—both surfaces infinite in radial extent—has been described using a scalar effective viscosity. A numerical shooting technique was used to obtain the flowfield for two cases, one having a gap Reynolds number of 296 (the "narrow" gap) and the other, 2852 (the "wide" gap), the radial distance covered in both cases corresponding to the radial Reynolds number range $0 \leqq R_e \leqq 10^7$.

Transition from laminar to turbulent flow was introduced gradually over the range $1.6 \times 10^5 \leqq R_e \leqq 2.5 \times 10^5$. The inner, laminar region is characterized by radially similar flow and constant-thickness boundary layers on disk and wall, as is well known. The turbulent layers, however, become thicker with radius, merging at a point determined by the gap width. For the narrow gap they were merged at all radii, while they were separate in the wide gap for $R_e \lesssim 2.56 \times 10^6$. The turbulent flows are essentially locally similar, i.e., the flows at different radii have little effect on each other. Thus the specification of the transition behavior has negligible effect on the turbulent flowfield at greater radii.

The foregoing approach yielded velocity profiles that agreed rather well with the small amount of experimental data available for an enclosed rotating disk configuration. The cylindrical enclosure of the tests does not appear to obstruct agreement with the present infinite-gap theory. Excellent agreement is obtained with the data for the integrated disk drag moment.

These results indicate that the fluid motion tends toward a two-dimensional, turbulent, Couette flow at large $R_e$. The narrow-gap results for the local coefficient of friction on the disk at large $R_e$ agree closely with that predicted by a relation derived for this asymptotic flow phenomenon.

## References

[1] Daily, J. W. and Nece, R. E., "Chamber Dimension Effects on Induced Flow and Frictional Resistance of Enclosed Rotating Disks," *Transactions of the ASME, Series D: Journal of Basic Engineering*, Vol. 82, 1960, pp. 217–232.

[2] Gregory, N., Stuart, J. T., and Walker, W. S., "On the Stability of Three-Dimensional Boundary Layers with Application to the Flow due to a Rotating Disk," *Philosophical Transactions of the Royal Society of London*, Vol. A248, 1955, pp. 155–199.

[3] Lance, G. N. and Rogers, M. H., "The Axially Symmetric Flow of a Viscous Fluid between Two Infinite Rotating Disks," *Proceedings of the Royal Society of London*, Vol. A266, 1962, pp. 109–121.

[4] Benton, E. R., "A Composite Ekman Boundary Layer Problem," Tellus, Vol. 20, No. 4, 1968, pp. 667–672.

[5] Reshotko, E. and Rosenthal, R. L., "Laminar Flow Between Two Infinite Disks, One Rotating and the Other Stationary," *Israel Journal of Technology*, Vol. 9, March 1971, pp. 93–103.

[6] Bondor, P., "Viscous Flow about an Enclosed Rotating Disk," Rept. No. FTAS/TR-69-39, March 1969, School of Engineering, Case Western Reserve Univ., Cleveland, Ohio.

[7] Ketola, H. N. and McGrew, J. M., "Pressure, Frictional Resistance and Flow Characteristics of the Partially Wetted Rotating Disk," *Transactions of the ASME, Series F: Journal of Lubrication Technology*, Vol. 90, April 1968, pp. 395–404.

[8] Bayley, F. J. and Owen, J. M., "Flow between a Rotating and a Stationary Disc," *The Aeronautical Quarterly*, Vol. 20, Pt. 4, Nov. 1969, pp. 333–354.

[9] Cooper, P., "Turbulent Boundary Layer on a Rotating Disk Calculated with an Effective Viscosity," *AIAA Journal*, Vol. 9, Feb. 1971, pp. 251–261.

[10] Cebeci, T. and Smith, A. M. O., "A Finite-Difference Solution of the Incompressible Turbulent Boundary Layer Equations by an Eddy-Viscosity Concept," Rept. DAC-67130, Oct. 1968, McDonnell Douglas Corp., Long Beach, Calif.

[11] Clauser, F. H., "The Turbulent Boundary Layer," *Advances in Applied Mechanics*, Vol. IV, Academic Press, New York, 1956, pp. 1–51.

[12] Cooper, P., "Turbulent Fluid Friction of Rotating Disks," Rept. FTAS/TR-72-82, Aug. 1972, Case Western Reserve Univ., Cleveland, Ohio; also CR-2284, July 1973, NASA.

[13] Bradshaw, P., "Calculation of Three-Dimensional Turbulent Boundary Layers," *Journal of Fluid Mechanics*, Vol. 46, Pt. 3, April 1971, pp. 417–445.

[14] Koosinlin, M. L. and Lockwood, F. C., "The Prediction of Axisymmetric Turbulent Swirling Boundary Layers," *AIAA Journal*, Vol. 12, April 1974, pp. 547–554.

[15] Coles, D., "The Law of the Wall in Turbulent Shear Flow," *50 Jahre Grenzschictforschung*, edited by H. Görtler and W. Tollmien, F. Vieweg und Sohn, Braunschweig, 1955, pp. 153–163.